Cancer Chemother Pharmacol (2012) 69:577–590
DOI 10.1007/s00280-011-1713-x

ORIGINAL ARTICLE

Pharmacodynamics of DT-IgG, a dual-targeting antibody against VEGF-EGFR, in tumor xenografted mice

Selwyn J. Hurwitz · Hongzheng Zhang · Sujin Yun · Thil D. Batuwangala · Michael Steward · Steve D. Holmes · Daniel Rycroft · Lin Pan · Mourad Tighiouart · Hyung Ju C. Shin · Lydia Koenig · Yuxiang Wang · Zhuo (Georgia) Chen · Dong M. Shin

Received: 6 December 2010 / Accepted: 15 July 2011 / Published online: 13 September 2011

Abstract
Purpose DT-IgG is a fully humanized dual-target therapeutic antibody being developed to simultaneously target epidermal growth factor receptor (EGFR) and vascular endothelial growth factor (VEGF), important signaling molecules for tumor growth. *The* antitumor pharmacodynamics (PD) of DT-IgG was studied in nude mice bearing human tumor xenografts with different EGFR and VEGF expressions and *K-ras* oncogene status and compared with bevacizumab, cetuximab and bevacizumab + cetuximab.

Methods Mice bearing human oral squamous cell carcinoma (Tu212), lung adenocarcinoma (A549), or colon cancer (GEO) subcutaneous xenografts were administered with the antibodies intraperitoneally (i.p.), and tumor volumes were measured versus time. Nonlinear mixed effects modeling (NONMEM) was used to study drug potencies (IC_{50}) and variations in tumor growth.
Results The PD models adequately described tumor responses for the antibody dose regimens. In vivo IC_{50} values varied with EGFR and *K-ras* status. DT-IgG had a similar serum $t_{1/2}$ as cetuximab ($\sim$1.7 vs. 1.5 day), was more rapid than bevacizumab ($\sim$6 day), and had the largest apparent distribution volume (DT-IgG > cetuximab > bevacizumab). The efficacy of DT-IgG was comparable to bevacizumab despite lower serum concentrations, but was less than bevacizumab + cetuximab.
Conclusions A lower IC_{50} of DT-IgG partially compensated for lower serum concentrations than bevacizumab and cetuximab, but may require higher doses for comparable efficacy as the combination. The model adequately predicted variations of tumor response at the DT-IgG doses tested and could be used for targeting specific tumor efficacies for future testing.

Keywords DT-IgG · Targeted antibody · EGFR · VEGF · Bevacizumab · Cetuximab · Pharmacokinetics · NONMEM · Tumor population pharmacodynamic model

Selwyn J. Hurwitz and Hongzheng Zhang contributed equally to this work.
Domantis Limited is a wholly owned subsidiary of GlaxoSmithKline.

S. J. Hurwitz (✉)
Center for AIDS Research, Laboratory of Biochemical Pharmacology, Department of Pediatrics, Emory University School of Medicine/VA Medical Center, Medical Research # 151H, 1670 Clairmont Road, Decatur, GA 30300, USA
e-mail: shurwit@emory.edu

H. Zhang · S. Yun · L. Koenig · Y. Wang · Z. Chen · D. M. Shin
Department of Hematology and Medical Oncology, Winship Cancer Institute, Emory University School of Medicine, Atlanta, GA, USA

T. D. Batuwangala · M. Steward · S. D. Holmes · D. Rycroft
Domantis Limited, 315 Cambridge Science Park, Cambridge, UK

L. Pan · M. Tighiouart
Department of Biostatistics, School of Public Health, Emory University, Atlanta, GA, USA

H. J. C. Shin
Quest Diagnostics, Atlanta, GA, USA

Introduction

Several humanized and chimeric monoclonal antibodies (MAbs) have been developed to target growth factor receptors involved in the vascularization and growth of solid tumors [1]. VEGF is an essential growth factor for

tumor vascularization and angiogenesis, which stimulates the growth of endothelial cells and increases vascular permeability [2]. The recombinant humanized IgG1 monoclonal antibody bevacizumab binds to the VEGF and inhibits its activity, thereby inhibiting angiogenesis and impeding tumor growth. Studies have established the benefits of combining bevacizumab with chemotherapy over monotherapy [3]. Bevacizumab is currently approved in combination with standard chemotherapy for the treatment of metastatic colon, non-small-cell lung and breast cancers. More recently, it has been used as a single agent for the treatment of glioblastoma multiforme with progressive disease following prior chemotherapy and surgery [4]. A recent large observational cohort study in metastatic colorectal cancer suggests an overall survival advantage of nearly 32 months in continuing bevacizumab [5, 6]. The clinical benefit of bevacizumab in metastatic colorectal cancer is independent of *K*-ras mutation status as shown by analysis of a phase III study of bevacizumab with chemotherapy in previously untreated metastatic colorectal cancer [7, 8]. The benefit of combining chemotherapy with bevacizumab is limited by the observed toxicities, which include hypertension (22–32% incidence in metastatic colorectal cancer), proteinuria and arterial thrombosis [9–14]. Further evidence of bevacizumab-induced toxicity has been observed in a recent study in engineered mice expressing humanized VEGF-A [15].

Overexpression of the epidermal growth factor receptor (EGFR) correlates with poor prognosis in individuals with head and neck, lung, breast, colon, and prostate cancers [16, 17]. The chimeric human–murine IgG1 antibody cetuximab binds to the external domain of EGFR, blocking phosphorylation to the active form, leading to receptor internalization and degradation [18]. Cetuximab is currently approved for the treatment of head and neck and colorectal cancer [19]. However, the presence of *K-ras* mutations has been associated with resistance to cetuximab and poor survival in patients with advanced colorectal cancer [20–22].

The VEGF and EGFR pathways are interconnected in promoting angiogenesis and tumor growth [23, 24], and positive outcomes of a phase I/II study with the combination of erlotinib and bevacizumab in HNSCC have supported the premise of targeting both EGFR and angiogenesis [25]. However, negative outcomes have been reported in studies involving the combination of bevacizumab and with either cetuximab [21] or panitumumab [26] in metastatic colorectal cancer, indicating the possibility of negative interaction between certain targeted antibodies. Furthermore, non-preferential delivery of anti-angiogenic agents may be responsible for their common side effects including hypertension, proteinuria, and bleeding [3, 13, 27, 28]. Therefore, there is a need for the development of new anti-angiogenic agents.

A dual-targeting antibody DT-IgG was developed by introducing anti-VEGF and anti-EGFR domain antibodies (dAbs) onto the heavy and light chains, respectively, of an IgG1 constant region to create a dual-targeting IgG (DT-IgG). This bispecific antibody could potentially act by blocking either angiogenesis and/or EGFR-dependent survival pathway, thereby targeting tumors regardless of *K-ras* mutation status. Since many tumors overexpress EGFR, this antibody could potentially lead to more specific binding of the chimeric antibody with the EGFR in these tumors, resulting in a preferential delivery of the anti-VEGF activity to the tumor bed than to non-tumor tissues with lower EGFR. This may result in a reduction in side effects secondary to non-specific VEGF inhibition, which have occurred in some trials with bevacizumab [13]. The use of a single dual-targeting antibody may also be easier to administer than separate molecules with differing pharmacokinetic (PK) profiles and could avoid possible interactions between two separate monoclonal antibodies [21]. Dual-targeting IgG antibodies have previously been studied. For example, Genentech has explored the therapeutic potential of an antibody targeting HER2 and VEGF, and its crystal structure has been revealed [29].

Tumor growth usually demonstrates Gomperzian-like kinetics, characterized by an initial exponential volume increase, followed by a linear growth phase and eventual plateauing to a pseudo-steady-state volume, which could result from tumors outgrowing their blood supply [30, 31]. Gomperzian models have been developed, which include the PK and pharmacodynamics (PD) of anticancer drugs for modeling responses in preclinical [32–37] and clinical [38] studies versus dosage regimen.

In this study, the tumor suppression of DT-IgG was compared with those of bevacizumab or cetuximab alone and in combination in mice bearing human tumor xenografts. A population PK-PD model based on a previous Gomperzian tumor kinetic model [34] was then fitted using a nonlinear mixed effects program (NONMEM 7.1, Ellicott City, MD), to study medians and variations in tumor growth inhibition of the tumor xenografts, as a function of their PK and potencies. The suitability of the population PK-PD model to predict variations in tumor response versus DT-IgG treatment was also tested, for use in the development of dose regimens for further preclinical studies.

Methods

Cell lines and reagents

Head and neck cancer (HNSCC) Tu212 cells were provided by Dr. Gary L. Clayman (MD Anderson Cancer

Center, Houston, TX) and were maintained in DMEM/F12 (1:1) medium supplemented with 5% heat-inactivated fetal bovine serum (FBS) in a 37°C, 5% CO_2 humidified incubator. A549 lung cancer cells were obtained from Dr. Shi-Yong Sun (Emory University, Atlanta, GA) and cultured in RPMI1640 with 10% FBS. GEO human colon cancer cells were obtained from Dr. Davide Melisi (MD Anderson Cancer Center—University of Texas) and were maintained in 5% DMEM medium. Cetuximab was obtained from ImClone (New York, NY) and bevacizumab from Genentech (San Francisco, CA).

Construction and production of the DT-IgG antibody targeting EGFR and VEGF

DT-IgG was constructed by grafting two independently selected human single-domain antibodies (dAbs) that bind VEGF and EGFR onto the constant region framework of human IgG1 using a previously published technique [39]. Briefly, the dAbs were selected using phage display techniques against recombinant VEGF (VH dAb) and recombinant human EGFR (Vk dAb) and were cloned in frame with the IgG1 heavy chain CH1-3 and light chain Ck coding regions in transient mammalian expression plasmids. To produce the DT-IgG, the individual plasmids expressing the EGFR and VEGF domains were co-transfected into HEK293/6E cells using conventional techniques in serum-free medium [40]. DT-IgG was purified from the culture supernatant by capture on a Stream Line Protein-A column (Amersham) followed by elution in 10 mM citrate (pH 3.0) and subsequent reformulation into 100 mM citrate (pH 6.0) with 10% PEG-300 and 5% sucrose. The approximate molecular weight of DT-IgG (145 kD) is similar to cetuximab (146 kD) and bevacizumab (149 kD).

Tumor xenograft studies

All studies were conducted after review by the GSK Institutional Animal Care and Use Committee and in accordance with the GSK Policy on the Care, Welfare, and Treatment of Laboratory Animals and were approved by the Institutional Animal Care and Use Committee (IACUC) of Emory University. Human tumor cells were inoculated into the flanks of 4–6-week-old athymic *nu/nu* mice (Taconic, NY) with 2.5×10^6 (TU212) or 5×10^6 (A549 and GEO) cells/mouse, respectively. The average weight of the mice was $\sim$20 g. Tumors were grown until they reached a volume of $\sim$125 mm^3 before initiating treatment with the various antibodies. The treatment dosages for Tu212 xenografts (starting on day 8 after implantation) were as follows: 1.25 mg/kg of IgG, bevacizumab, cetuximab or a combination of bevacizumab with cetuximab, once/week; DT-IgG at 0.625 mg/kg twice/week ($n = 7$), 1.25 mg/kg twice/week ($n = 7$), or 1.25 mg/kg once/week ($n = 8$) for 29 days. The dosages for A549 xenografts (commencing on day 8 after implantation) were as follows: 2.5 mg/kg twice/week ($n = 9$/treatment group) IgG, bevacizumab, cetuximab, bevacizumab + cetuximab or DT-IgG intraperitoneally (i.p.) for 31 days. The dosages of the various antibodies for GEO xenografts (commencing on day 7 after implantation) were 2.5 mg/kg twice/week for 26 days ($n = 8$/treatment group). Tumors were measured three times a week, and volumes (V) were calculated using the formula:

$$V = \pi/6 \times \text{larger diameter} \times (\text{smaller diameter})^2, \quad (1)$$

as reported previously [41]. Animals were observed daily for clinical signs of toxicity and weighed twice per week. Mice were killed at the end of experiment or when tumor diameters reached 2 cm in diameter. Tumor volumes versus time profiles were obtained in all animals.

Statistical comparison of relative potencies of antibodies within cell lines

The tumor growth kinetics of mice bearing Tu212, GEO, and A549 xenografts, treated twice per week with IgG, DT-IgG, bevacizumab, and cetuximab were subjected to statistical analysis. Mice bearing Tu212 xenografts received 1.25 mg/kg of antibody twice per week, while those bearing GEO and A549 xenografts received 2.5 mg/kg of antibody twice per week (Fig. 1). Tumor growth kinetics of each cell line was compared versus treatment using general linear mixed modeling. Type of treatment and time of measurement and their interactions were included in the model as fixed effects. Assumptions used in the analysis included compound symmetry (CS), autoregressive (AR(1)), Type H (HF), unstructured (UN), and variance component (VC). In each case, the best model was selected based on a likelihood ratio test for nested models using Akaike and Bayesian information (AIC/BIC) criteria for non-nested models. Pair-wise comparisons of mean differences between the estimated least square means of the various treatments were performed using a student t test, with a Bonferroni correction for multiple comparisons. A P-value of <0.05 was considered significant. Analyses were performed using the SAS statistical program (ver. 9.2, Carey, NC).

Serum PK

The single dose of DT-IgG was studied in female BALB/c mice injected i.p. with a 5 mg/kg body weight dosage of DT-IgG. Blood samples were collected at 0 (pre-dose) and 12, 24, and 48 h post-administration by cardiac puncture

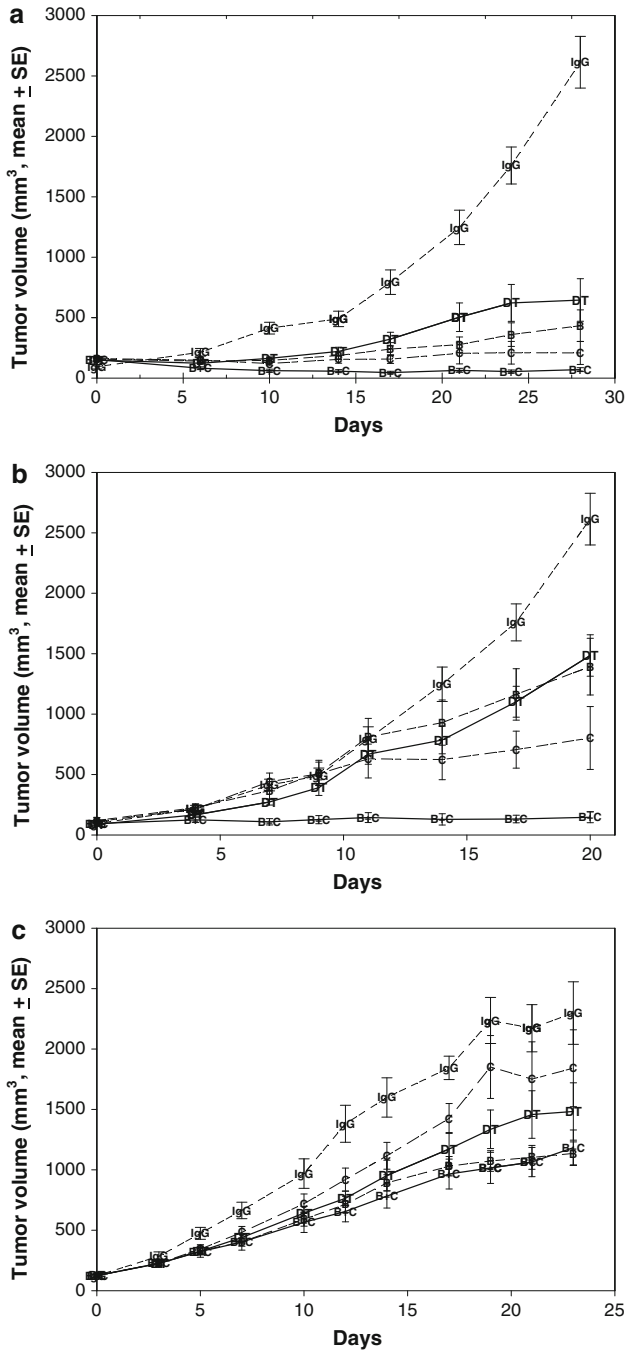

Fig. 1 Plot of mean tumor volume (±standard error of the mean, SE) in nude mice bearing the following: human Tu212 oral small-cell carcinoma (**a**), GEO colon cancer (**b**), and A549 alveolar adenocarcinoma (**c**) tumor xenografts. Mice were administered ip. injections of IgG (*IgG*), DT-IgG (*DT*), bevacizumab (*B*), cetuximab (*C*) and the bevacizumab + cetuximab combination (*B*+*C*). Mice bearing Tu212 xenografts received 1.25 mg/kg of antibody twice per week, while those bearing GEO and A549 xenografts received 2.5 mg/kg of antibody twice per week

($n = 3$/time point). Serum was separated and assayed for DT-IgG using recombinant human EGFR (extracellular domain) and a VEGF capture ELISA. Detection was performed using an anti-human IgG1-horseradish peroxidase-conjugated polyclonal antiserum and the substrate tetramethylbenzidine.

The rate of decline in DT-IgG (dC_p/dt) appeared mono-exponential. Therefore, serum concentrations (C_p) versus time profiles were fitted to a one-compartment PK model, assuming bolus input into the central compartment using the equation:

$$dC_p/dt = -D/V_d k_e \quad (2)$$

In this expression, D the i.p. dose, V_d is the apparent volume of distribution, and k_e the elimination rate constant.

The average PK parameters of bevacizumab and cetuximab in mice after i.p. administration were obtained from previous studies [42, 43]. Bevacizumab was assumed to have an absorption rate constant from the peritoneal compartment of 5.79 per day (0.241 per h) and 92.8% systemic bioavailability. The average respective volumes of distribution and clearance values of the central and peripheral compartments were 49.4 and 53.8 ml/kg and 6.27 and 87 ml/kg per day, respectively, and the terminal elimination half-life ($t_{1/2}$) was 5.5 day. [42]. The cetuximab was absorbed into the serum compartment with a first-order rate constant of 0.44 per h after i.p. administration and eliminated with a rate constant of 0.017 per h (corresponding to a $t_{1/2}$ of $\sim$1.7 day). The apparent systemic volume of distribution of cetuximab was 94 ml/kg [43].

Average PK parameters of DT-IgG, bevacizumab and cetuximab were used for all simulations (Fig. 2) and for PD modeling. The PK models did not consider the effect of antibody binding and internalization on the systemic clearance, as tumors increase in size [44]. The use of average parameters assumes that the contribution of variations in PK had minimal effect on tumor PD compared to other variance sources.

Tumor PD

Mixed effect modeling was used to quantify the variations in tumor growth, using the NONMEM computer program (version 7.1, ICON Development Solutions, Ellicott City, MD) [45, 46]. NONMEM was run under the PLT tools graphical interface and project controller (version 2.5, PLTsoft, San Francisco, CA). The Fortran compiler was GFORTRAN Windows (ver. 460, GNU Free Software Foundation, Boston, MA).

The PK-PD relationship between Cp and antitumor growth efficacy (E) was modeled using the Hill equation:

$$E = (C_p^{\eta}/\mathrm{IC}_{50}^{\eta} + C_p^{\eta}) \quad (3)$$

Equation 3 assumes that the therapeutic antibody was present in the serum at levels much higher than the receptors and binds rapidly and competitively with EGFR

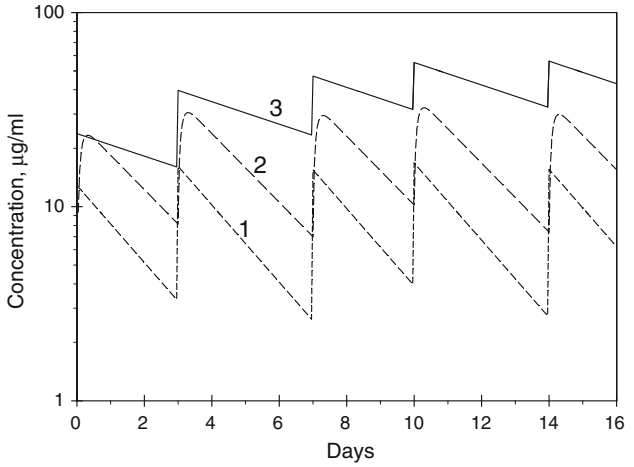

Fig. 2 Simulated average serum concentrations of DT-IgG (*1*), cetuximab (*2*) and bevacizumab (*3*) in nude mice administered 2.5 mg/kg antibody (i.p.) twice a week (e.g., Friday and Monday). The average systemic clearance (CL/F) and volume of distribution (V/F) of DT-IgG were 0.089 l/kg/day and 0.194 l/kg, respectively. The average two-compartment and one-compartment PD parameters of bevacizumab and cetuximab, respectively, in nude mice after i.p. administration were obtained from previous studies and used unchanged in the simulation [42, 43]

and/or VEGF, directly inhibiting biological activity. It was also assumed that the rate of turnover of the receptor complex was much slower than the association and dissociation rates.

The available data did not allow partitioning of drug effect between the occupancy of DT-IgG to the individual EGFR and VEGF, respectively. IC_{50} and (η) represent the median serum concentration needed for 50% inhibition of cell growth and Hill concentration exponent, respectively. These values were considered cell line dependent, as they rely on the density and ratio of EGFR and VEGF associated with the cell. The volume of the tumor was assumed to be small enough such that the fraction of DT-IgG partitioning into and binding with receptors in the tumors would not appreciably affect the V_d of the drug. It was also assumed that the turnover of the receptor complex would not affect the serum PK of DT-IgG.

The rate of tumor growth was modeled as:

$$dV/dt = [L_0 * V/(1 + (L_0/L_1 * V)^{\Psi})^{1/\Psi}) - V(k_{pl} + k_{Dpl}E)](1 - E) \quad (4)$$

Equation 4 was simplified from a previous model [34] for cytotoxic drugs, under the assumption that growth inhibition of the dividing cell fraction in the tumor is directly related to binding of DT-IgG with EGFR and VEGF. L_0 is the initial exponential phase rate constant, which is dominant before the tumor growth transitions to a pseudo-linear phase (growth rate L_1). The steepness of transition from exponential to linear growth is modeled by the parameter ψ. Tumor growth eventually plateaus to a maximal volume, influenced by k_{pl}. Since DT-IgG acts as an inhibitor of EGFR and VEGF, reduction in the rate of both growth and plateau volume was considered related to E. Therefore, the model also incorporated the coefficient k_{Dpl}, which models any further drug-related decrease in tumor plateau volume, proportional to E.

The variation in growth constants (L_0 and L_1) of tumors between animals inoculated with the same tumor cell line were assumed to be log-normally distributed and was modeled using equations similar to Eq. 5 (for L_0):

$$L_0, L_{0,i} = L_{0,\text{typical}} \times e^{(\eta i)}, \quad (5)$$

where $L_{0,i}$ is the L_0 for the ith individual, η_i is the population inter-individual variation with a mean of 0 and variance ω^2. $L_{0,\text{ typical}}$ is the value for the population estimate (no variation) of L_0.

An exponential residual error model of tumor volume was implemented by fitting the model to log-transformed data, using the error structure

$$Y = F + \text{EPS}_1, \quad (6)$$

where EPS_1 was assumed normally distributed with mean 0 and variance σ^2. Therefore, predicted tumor volumes were obtained by exponentiation of the output. Due to large variations in tumor growth parameters and relatively small sample sizes, standard errors were computed using the COVARIANCE and MATRIX = S options in NONLIN [45]. Individual Bayesian estimates of the model parameters were calculated using the POSTHOC option in NONMEM.

PD model diagnostics and validation

Goodness of fit for the various models was assessed based on the examination of the following: achievement of model convergence with parameter estimates (preferably to >two significant places), examination of the objective function obtained from the NONMEM output (equivalent to the $-2 \times$ log-likelihood function), noting that a smaller value corresponds to a better model fit to the data; and visual diagnostics—visual diagnostics included examination of the symmetry and dispersion of the ratio of observed/predicted tumor volumes (population and post hoc predictions) versus time for each cohort, noting that a perfect fit would produce observed/predicted ratios equal unity for all time periods (Fig. 3). A visual predictive check was performed as an internal model validation, to test the ability of the fitted models to predict the actual tumor volumes versus time profiles during treatment with the various therapeutic antibodies [45]. This involved using the models fitted to simulate 1,000 theoretical tumors for each dose regimen and calculating 5th, 25th, median, 75th and 95th percentile ranges, were then plotted versus time, and superimposed

over the experimental observations, for comparison (Fig. 4a i–iii for Tu212, 4b for GEO, and 4c for A549 xenografts). A visual predictive check was also used to perform an external validation using data from animals bearing Tu212 xenografts, since that cohort contained the most extensive data ($n = 28$ xenografts, from four treatment regimens (including IgG control), comprising 218 observations). This involved fitting a model to the twice a week doses of DT-IgG and IgG cohorts (0, 0.625, and 1.25 mg/kg), and using the model to simulate tumor volumes versus time profiles for mice treated with 1.25 mg/kg once per week, and comparing predications to actual observations (Fig. 4a iv).

Comparison of PD between therapeutic antibodies

Separate PD models were fitted for tumors derived from each cell line. Models were initially fitted using the combined tumor data from mice treated with DT-IgG and control) IgG (step A). To allow comparison with other therapeutic antibodies, models were then refitted to data from animals treated with bevacizumab and cetuximab (step B). During step B, the parameters fitted in step A were held constant; however, the IIV of L_0 and L_1 were allowed to vary. Concentration exponents (γ) for bevacizumab and cetuximab were assumed equal to 1, since limited data were available for those treatments. Xenografts treated with the

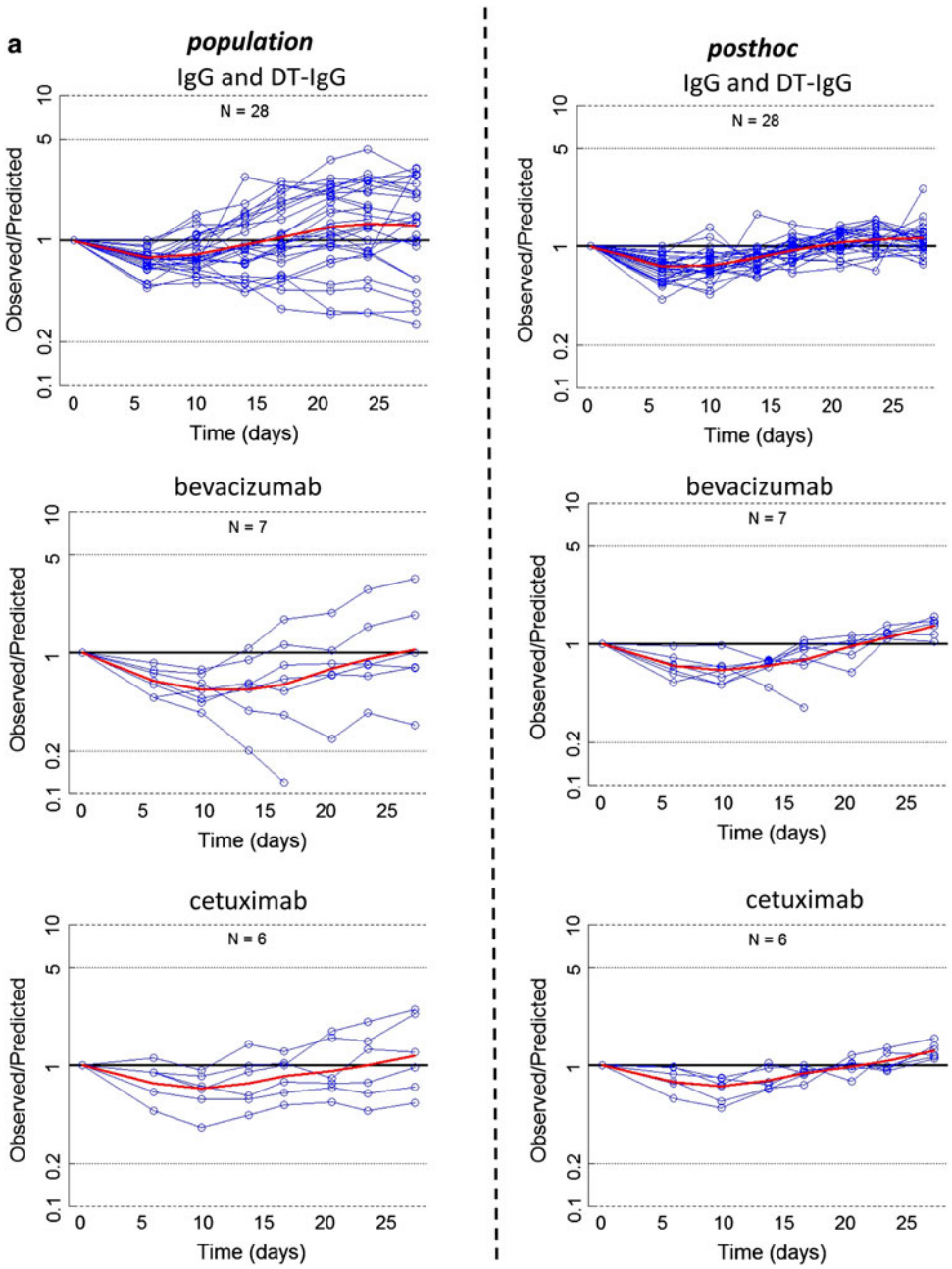

Fig. 3 Goodness of fit diagnostic plots for the various models: **a** Tu212 HNSCC, **b** GEO colon cancer and **c** A549 lung adenocarcinoma. Ratios of observed tumor volumes divided by volumes predicted by the pharmacodynamic model were plotted versus time for each mouse. Also listed are the number of tumor bearing mice included in each analysis. The *left panels* are based on the "typical" prediction without including model variability (population fit), while the *right panels* are based on the complete model including inter-individual variability (IIV) (post hoc fit). The curvilinear plots depict local regression smoother (LOESS). If the model fitted the data perfectly, *all lines* would lie *horizontally* at 1.0. Inclusion of the error model (population vs. ad hoc model) decreased the standard errors of prediction for the Tu212 cohorts treated with IgG or DT-IgG, bevacizumab and cetuximab decreased from 29 to 1 6%, 35 to 21%, and 29 to 13%, respectively; Similarly, the decrease in standard errors of prediction for the GEO tumors were 28–10%, 24–7%, and 38–12%, respectively, while the decrease in standard error of prediction for the A549 cohorts were from 12 to 5%, 15 to 10%, and 18 to 9%, respectively. Improved fit with the post *hoc* models is expected because they include IIV

Fig. 3 continued

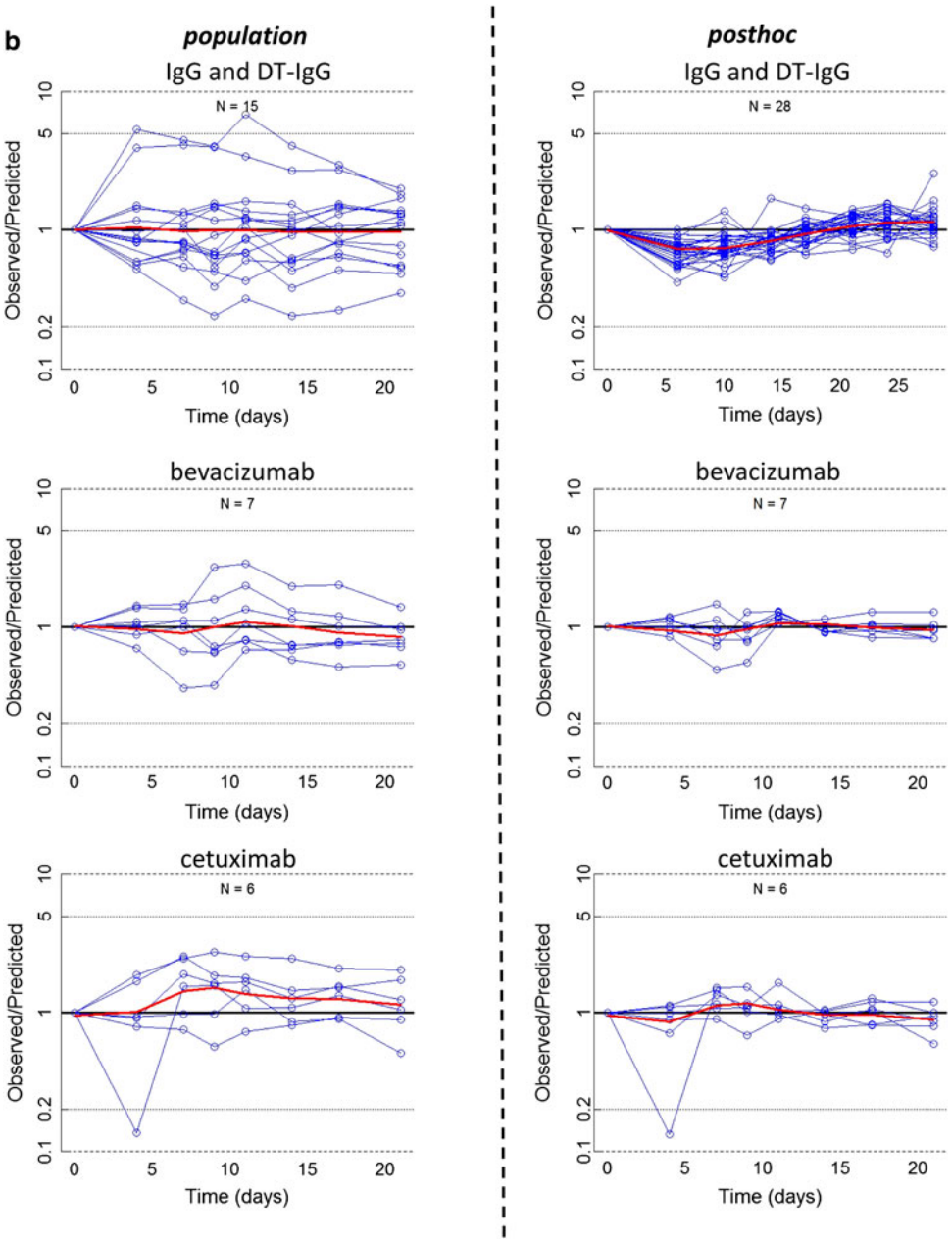

bevacizumab + cetuximab combination were not modeled due to insufficient data.

Results

Statistical comparison of the growth kinetics tumor xenografts

Tu212, A549 and GEO xenografts were grown in the flanks of nude mice. The volumes of these tumors were plotted versus time from mice treated with IgG, DT-IgG, or bevacizumab and cetuximab alone or in combination and are shown in Fig. 1. The doses of antibodies administered i.p. to mice bearing Tu212 xenografts were 1.25 mg/kg, while mice bearing GEO and A549 xenografts received 2.5 mg/kg twice per week. All treatments suppressed tumor growth significantly compared to the IgG control in Tu212 xenografts ($P < 0.0001$). DT-IgG inhibited tumor growth, to a similar degree as bevacizumab, but was less potent compared with cetuximab ($P < 0.026$) or the combination of bevacizumab and cetuximab ($P < 0.0008$). In the case of GEO and A549 xenografts, DT-IgG demonstrated similar efficacy to bevacizumab and cetuximab alone. However, the combination of bevacizumab and cetuximab was more efficacious than the other treatments ($P < 0.0001$). A

Fig. 3 continued

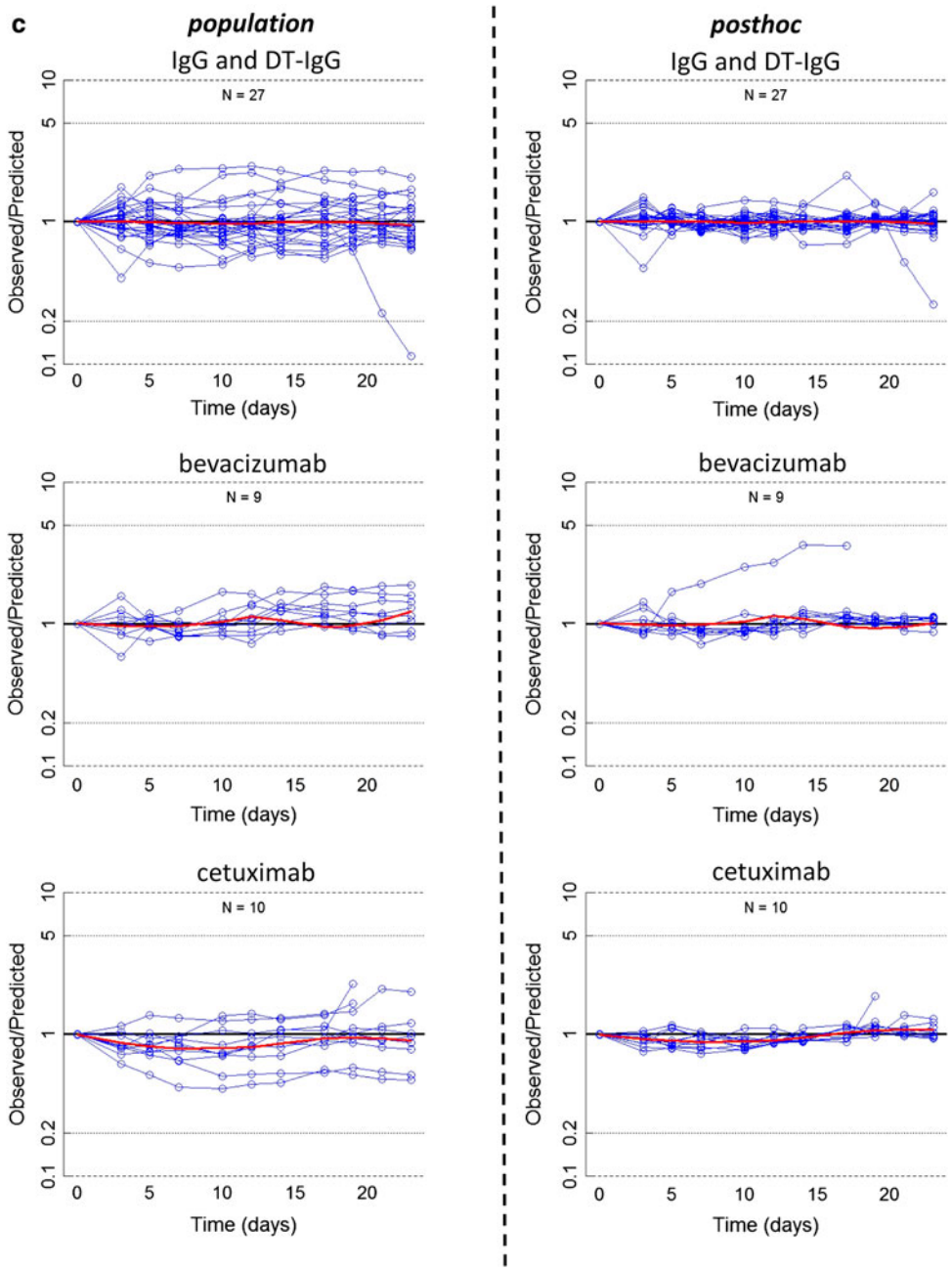

dose-dependent decrease in median tumor growth was observed for Tu212 and A549 tumors treated with the various dose regimens of DT-IgG. However, a large degree of variability and substantial overlap was observed in tumor volumes of cohorts treated with the various doses of DT-IgG.

PK of DT-IgG

Serum concentrations of DT-IgG were fitted to a one-compartment model since data were only available post absorption following i.p. administration and declined mono-exponentially. The average systemic clearance (CL/F) and volume of distribution (*V/F*) of DT-IgG were 0.089 l/kg/day and 0.194 l/kg, respectively.

Predicted serum concentrations of DT-IgG, cetuximab, and bevacizumab following twice a week i.p. administration at 2.5 mg/kg i.p. doses per antibody in nude mice are plotted in Fig. 2. The predicted accumulation of bevacizumab in serum was markedly higher for bevacizumab than for DT-IgG or cetuximab, due to its smaller apparent distribution volume and longer $t_{1/2}$ than the other antibodies. Although the serum $t_{1/2}$ of DT-IgG and cetuximab was similar, serum concentrations of DT-IgG were lower,

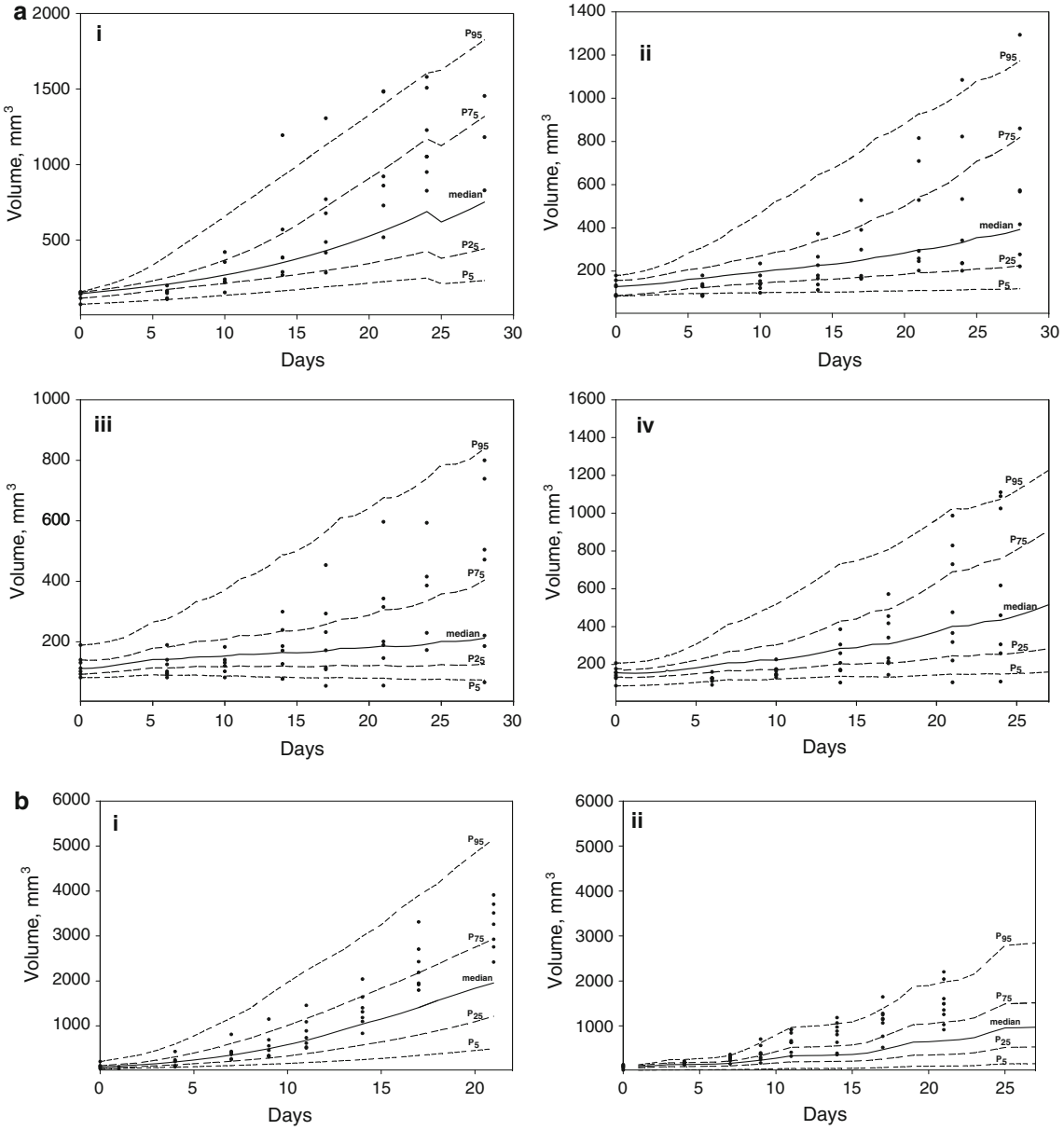

Fig. 4 Model validation by "visual predictive check," performed on the DT PD models of tumor volume of xenografts versus time and DT-IgG treatment regimen in nude mice bearing: Tu212 tumors (**a**) treated with IgG (*i*), 0.625 mg/kg DT-IgG twice per week (*ii*), or 1.25 mg/kg DT-IgG twice per week (*iii*). As an external model validation, the tumor growth rate of during 1.25 mg/kg once per week regimen was simulated using the model fitted using only data from mice receiving twice a week DT-igG and compared with actual data (*iv*). Similar internal validations were performed for GEO tumors (**b**) treated with IgG (*ii*) or 2.5 mg/kg DT-IgG twice per week (*ii*), and A549 tumors (**c**) treated with IgG (*i*), 2.5 mg/kg DT-IgG once per week (*ii*) or 10 mg/kg DT-IgG twice per week (*iii*). One thousand simulations were performed for each treatment regimen to calculate and percentiles (P_5, P_{25}, P_{50}, P_{75} and P_{95}) of tumor volume versus time. The actual observations were superimposed over these ranges for comparison

suggesting that DT-IgG has a larger apparent volume of distribution.

Tumor PD modeling

A cytotoxic model that assumed direct killing of dividing cells by the therapeutic antibodies [34] did not converge and was rejected in favor of the growth inhibition model (data not shown). The population PD parameters fitted to describe the growth of the various tumor xenografts during treatment with DT-IgG, bevacizumab, cetuximab and the IgG antibodies are summarized in Table 1. The respective relative standard errors (RSE, %) were included in the table when they were included in the NONMEM output.

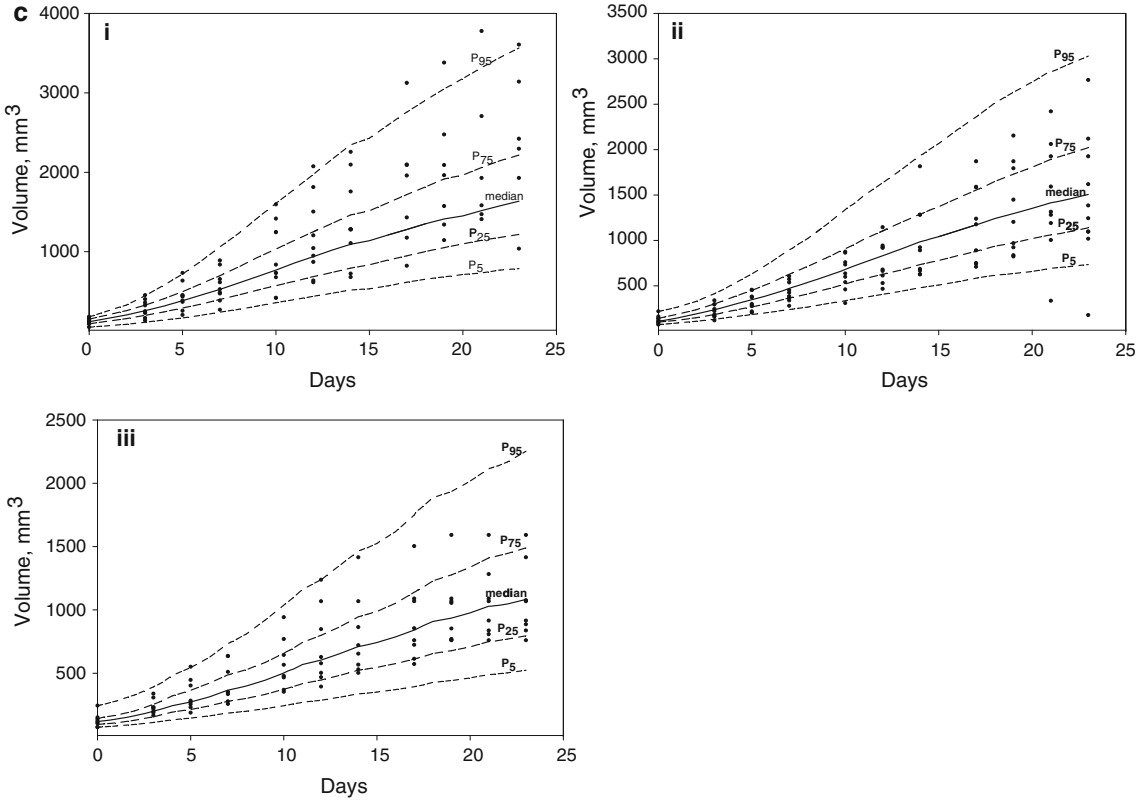

Fig. 4 continued

Inter-subject variations (IIV) were estimated for L_0 and L_1 and were reported as % coefficients of variation (% CV), noting that the % CV for log-normal distribution = $\sqrt{(e\text{^}\omega^2 - 1)} \times 100$, where ω^2 is the lognormal variance. The RSE reported for IIV were for ω.

The model described tumor growth satisfactorily for animals treated with IgG and DT-IgG (step A) and converged to >2.3 decimal places. The IC_{50} of DT-IgG versus Tu212, GEO, and A549 were 12, 30.5, and 85 μg/ml, respectively. IIV of L_0 and L_1 indicated marked intrinsic variability in tumor kinetics of the various xenografts. A549 and GEO tumors had faster linear growth rates than Tu212 (200 and 161 vs. 66.1 mm^3/day, respectively), and Tu212 demonstrated a more abrupt transition (ψ = 14.9), than GEO (6.67), or A549 (1.47) xenografts. The predicted effect of DT-IgG on reducing plateau tumor volume (modeled by k_{Dpl}) was greater for Tu212 than for A549 or GEO xenografts (k_{DPL} = 0.15, vs. and 1.4×10^{-3} and 4.7×10^{-5} (negligible), per day ng/ml, respectively). Plateauing of tumor growth with size independent of drug (k_{pl}) was more apparent with A549 than with Tu212 or GEO xenografts (6.9×10^{-3} vs. 1×10^{-3} and 4×10^{-4}, per mm^3/day, respectively. Models fitted to the bevacizumab and cetuximab data (modeling step B) converged to fewer decimal places than the models fitted in step A. The models of Tu212 xenografts treated with bevacizumab and cetuximab did not converge to 2 decimal places. Therefore, these IC_{50} values should be considered approximate. The cetuximab IC_{50} values fitted for GEO, Tu212, and A549 were 87.5, 135, and >17,000 μg/ml, in concert with their EGFR and K-*ras* status. The corresponding IC_{50} values of bevacizumab were 126, 119, and 140, respectively.

The observed/predicted ratios (population and post hoc) for tumor volumes of Tu212, GEO, and A549 xenografts versus time were plotted in Fig. 3a, b, and c, respectively. The dispersion of the ratios about the x-axis is a measure of deviation of the model from the observed data. A local regression smoother (LOWESS) was also included in each plot. The errors of prediction for the DT-IgG models were reduced by inclusion of IIV for L_0 and L_1, and the median predicted errors were reduced from 29 to 16%, 34 to 10%, and 12 to 5%, for the Tu212, GEO, and A549 models, respectively. Likewise, the errors of prediction of bevacizumab and cetuximab were reduced by inclusion of variations in the model. The improved fit with the post hoc model is expected because that approach permits IIV [47]. Overall, the diagnostic curves suggest that the model described the tumor volumes versus time profiles adequately, although there was a trend toward underestimation

Table 1 Tumor growth and pharmacodynamic parameters

Model step A Estimate (RSE, %)	Tu212 oral squamous carcinoma (elevated EGFR, *wt Kras*)		GEO colon cancer (low EGFR, *wt K-ras*)	A549 lung adenocarcinoma (low EGFR, *mut K-ras*)
	(2× per wk group)	(all groups)		
Parameters fitted for DT-IgG				
IC_{50} (μg/ml)	12 (44.5)	12 (0.3)	30.5[a]	85 (58.4)
γ	1 (68.0)	1 (48.0)	0.96[a]	0.94 (70.2)
L_0, (exponential, day^{-1})	0.075 (36.0)	0.075 (26.7)	0.196 (20.4)	0.371 (14.6)
L_1,(linear, mm^3/day)	66.3 (40.1)	66.1 (20.0)	161 (36.3)	200 (0.002)
k_{Dpl} $(day\ ng/ml)^{-1}$	0.15 (58.0)	0.15 (33.3)	4.7×10^{-5}[a]	0.0014[a]
k_{pl} $(day)^{-1}$	1.0×10^{-3}[a]	1×10^{-3} (0.03)	4.14×10^{-4}[a]	6.9×10^{-3} (20.5)
ψ	14.9[a]	14.2[a]	6.67[a]	1.47 (27.9)
IIV L_0 (%)[d]	58 (43)	58 (16)	51.8 (28)	30 (46)
IIV L_1 (%)[d]	10[a]	10[a]	59.6 (100)	49 (39)
σ^2 (mm^3)	0.072 (1.3)	0.071 (1.4)	0.037 (35.1)	0.026 (2.8)
−2 × log likelihood	−177	−234	−187	−734
Significant digits	2.3	2.3	3.0	3.1

Model step B Estimate (RSE, %)	Tu212 model A, co-fitted to bev[c]	Tu212 model A, co-fitted to cet[c]	GEO model A, co-fitted to both bev and cet	A549 model A, co-fitted to both bev and cet
Tumors treated with bevacizumab (bev) and cetuximab (cet)				
IC_{50} of bev (μg/ml)	119[a]		126 (36.5)	140 (37.1)
IC_{50} of cet (μg/ml)		135[a]	87.5 (38.9)	>17,000[a]
γ for cet and bev[b]	[b] 1	1	1	1
IIV L_0 (%)[d]	74 [a]	54[a]	41.5 (12)	16 (25)
IIV L_1 (%)[d]	13[a]	14[a]	36 (20)	49 (25)
σ^2 (mm^3)	0.10[a]	0.09[a]	0.064 (4.7)	0.12 (2.3)
−2 × Log likelihood	−263	−300	−280	−426
Significant digits	<1	<1	2.3	2.3

Median inhibitory concentrations (IC_{50}), concentration exponents (γ) of DT-IgG, as well as tumor growth modeling constants describing the exponential (L_0) and linear (L_1) phases of tumor growth, steepness of transition from exponential to linear tumor growth (ψ), and drug-dependent (k_{Dpl}) and drug-independent (k_p) decrease in plateau volumes of the various tumors, were derived by co-fitting tumor volumes versus time profiles of mice treated with DT-IgG and IgG (control), (models A). IC_{50} and γ of bevacizumab (bev) and cetuximab (cet) were obtained by refitting the model to the entire data set for the respective tumors, holding the IC_{50} and γ fitted in A constant (models B). IIV of L_0 and L_1 were allowed to vary when fitting models B. Since tumor volumes were assumed to be distributed log-normally, log-transformed tumor volumes were used in the model fitting. Therefore, predicted tumor volumes were obtained by exponentiation of the dependent variable

[a] RSE were not reported if >parameter estimate

[b] γ fixed to 1 in model

[c] The IC_{50} of bevacizumab and cetuximab in Tu212 cells were fitted separately, since when combined, the model was unable to converge

[d] IIV of L_0 and L_1 were reported as % RSE, noting that % CV for log-normal distributed parameters $= \sqrt{(e\hat{}\omega^2 - 1)} \times 100$, where ω^2 = variance. The % RSE reported for IIV were for the estimate of ω. PD models were fitted using NONMEM ver. 7.1. The approximate molecular weights of DT-IgG, cetuximab, and bevacizumab are 145, 146, and 149 kD, respectively

of Tu212 and GEO tumor volumes during the first 5 days of the experiment when tumors were small.

Model validation

Figure 4a i–iii contain plots of simulated percentile ranges (P_5, P_{25}, median, P_{75}, P_{95}) of Tu212 tumor volumes versus time predicted by the full model assuming dosages of 0.625, 1.25 mg/kg twice per week, respectively. The corresponding curve for 1.25 mg/kg DT-IgG once per week (iv) represents an external validate, since the percentile ranges were simulated using the model fitted using only the IgG twice per week DT-IgG regimen. Internal "visual predictive check" validations of GEO tumors treated with IgG and 2.5 mg/kg are summarized in Fig. 4b i and ii, respectively, while those for A549 tumors treated with IgG, 2.5 or 10 mg/kg of DT-IgG, are summarized in Fig. 4c i–iii. The data spread about the predicted

percentiles of the various tumor xenografts in mice treated with the various treatments, suggests that the model adequately mimicked the experimental data. However, the variations in tumor sizes were over-predicted for the GEO tumors, which could have resulted from data limitations, as only data from IgG (control) and DT-IgG 2.5 mg twice per week treatments were available to fit the GEO xenograft model.

Discussion

DT-IgG is a fully humanized dual IgG antibody being developed to simultaneously target EGFR and VEGF, respectively) which, once activated, stimulate the growth of many tumors. In this study, we compared the efficacy of DT-IgG with that of bevacizumab which targets VEGF, cetuximab which targets EGFR individually and with the bevacizumab + cetuximab combination, each administered i.p. at the same dosages to athymic immunocompromised (*nu–nu*) mice bearing human xenografts. Tumor xenografts tested were comprised of Tu212, a HNSCC which express high levels of EGFR and have wild-type (wt) *K-ras*; GEO colon cancer cells that express low levels of EGFR and have *K-ras*-wt; and NSCLC A549 cells expressing low levels of EGFR and mutated (mut) K-ras. Statistical analysis indicated DT-IgG produced similar efficacy compared with bevacizumab in all tumors tested, but was less efficacious than cetuximab in Tu212 xenografts. All monotherapies were less efficacious than bevacizumab + cetuximab, and all therapeutic antibodies were more efficacious than the IgG control treatment.

Comparison of predicted serum concentrations of the therapeutic antibodies administered at the 2.5 mg/kg i.p. twice per week (Fig. 2) indicated that bevacizumab produced higher serum concentrations and demonstrated greater accumulation between doses than the other agents, due the longer $t_{1/2}$ (5.5 day vs. ~1.7 day for cetuximab and DT-IgG), and a smaller apparent V_d. A larger apparent V_d may be expected for DT-IgG, since DT-IgG targets both EGFR and VEGF. Therefore, the spectrum of tissues binding either anti-EGFR or VEGF could be greater than those binding to only one. The bound fraction of antibody is removed from serum, leading to a larger estimate of V_d. Interestingly, the V_d reported for cetuximab was greater than that of bevacizumab [42, 43], which could suggest a greater extent of antibody binding for cetuximab. However, the antibodies were administered i.p., so that differences in V_d could also be due to differences in tissue binding in the peritoneal cavity, resulting in an altered fraction of antibody reaching the systemic circulation. The similar $t_{1/2}$ of DT-IgG to cetuximab suggests that the dose frequency of DT-IgG could be similar to cetuximab, provided adequate post-infusion serum concentrations are achieved. PK-PD modeling was used to further explore the efficacy of DT-IgG.

The growth of tumor xenografts is intrinsically variable and difficult to control experimentally [48, 49]. Therefore, a NONMEM model was used to model the PD parameters and the IIV in the growth kinetics among xenografts of the same cell lines. This modeling approach produces a median response curve analogous to geometric mean response (population fit) and a post hoc prediction for each tumor based on the fitted parameters and variance structure (post hoc response) [38, 45, 46]. The inclusion of inter-individual variance (IIV) of growth constants L_0 and L_1 adequately described tumor variations to treatment with the therapeutic antibodies (Fig. 1). Antitumor activities were modeled using a tumor growth inhibition model, since inhibition of VEGF and EGFR are not directly cytotoxic, and a cytotoxic model [33] did not describe the data adequately.

The in vivo serum IC_{50} of DT-IgG indicated greater potency versus Tu212 than GEO or A549 (IC_{50} = 12, 30.5, and 85 μg/ml, respectively) in accordance with the *K-ras* and EGFR status of the various cell lines. Likewise, the IC_{50} of GEO, Tu212, and A549 increased in accordance with EGFR and K-*ras* status. However, differences in bevacizumab IC_{50} between xenografts were less substantial (119–140 μg/ml). In all cases, the in vivo IC_{50} of DT-IgG was lower than that of bevacizumab and cetuximab (Table 1).

The effect of dose frequency on tumor response was assessed by comparing simulated percentile ranges of tumor volume versus time, relative to predicted serum concentration of DT-IgG administered at 0.625 mg/kg twice per week and 1.25 mg/kg once per week regimens, respectively. The superior response observed at 0.625 mg twice per week may be explained by the higher predicted steady-state serum concentration than at the 1.25 mg once a day regimen. This suggests that it may be prudent to avoid the low trough levels of DT-IgG observed with the once a week dosage, which could allow tumor growth to recover toward the end of the dose interval.

The DT-IgG models fitted percentile ranges (P_5, P_{25}, P_{50}, and P_{95}) of tumor volume versus time were in agreement with the actual Tu212 and A549 data, but over-predicted the volume ranges for GEO tumors, probably as a result of limited data for the GEO xenografts (Fig. 3c). Furthermore, the model fitted using Tu212 data from twice per week DT-IgG treatment regimens successfully predicted the percentile ranges for the of tumor volume versus time for the 1.25 mg/kg once per week cohort. Therefore, the model could be applied to design dose regimens based on targeted tumor responses for further preclinical development of DT-IgG.

In summary, this analysis suggest that that DT-IgG had a lower in vivo IC_{50} compared with the other antibodies tested, which partially compensated for lower serum concentrations. However, larger DT-IgG doses are needed to produce efficacies similar to bevacizumab + cetuximab. A $t_{1/2}$ similar to cetuximab suggests that provided suitable post-infusion serum concentrations are achieved, DT-IgG may be suitable for once per week administration since cetuximab is typically administered once per week and has been considered for biweekly administration for the treatment of colorectal neoplasms [50]. Furthermore, using a bifunctional antibody similar to DT-IgG would avoid dosing complications arising from co-administration of bevacizumab and cetuximab which have markedly different PK profiles. The model successfully predicted tumor responses for DT-IgG versus dose and could be used to design treatment regimens that target specific antitumor efficacies for further preclinical testing.

Acknowledgments This study was funded by Domantis (a wholly owned subsidiary of GlaxoSmithKline), which also provided DT-IgG. Domantis (GSK) did not interfere with the pharmacodynamic aspects of the study such as experimental design, data collection, interpretation, modeling, decision to publish, or manuscript preparation. Dr. Hyung Ju C Shin, a pathologist for Quest Diagnostics, has kindly offered her expertise in these studies without any financial compensation from Winship Cancer Institute.

References

1. Argyriou AA, Kalofonos HP (2009) Recent advances relating to the clinical application of naked monoclonal antibodies in solid tumors. Mol Med 15(5–6):183–191
2. Cuevas I, Boudreau N (2009) Managing tumor angiogenesis: lessons from VEGF-resistant tumors and wounds. Adv Cancer Res 103:25–42
3. Ellis LM, Rosen L, Gordon MS (2006) Overview of anti-VEGF therapy and angiogenesis. Part 1: angiogenesis inhibition in solid tumor malignancies. Clin Adv Hematol Oncol 4(1):suppl 1–10
4. Cohen MH, Shen YL, Keegan P, Pazdur R (2009) FDA drug approval summary: bevacizumab (Avastin) as treatment of recurrent glioblastoma multiforme. Oncologist 14(11):1131–1138
5. Grothey A, Sugrue MM, Purdie DM, Dong W, Sargent D, Hedrick E, Kozloff M (2008) Bevacizumab beyond first progression is associated with prolonged overall survival in metastatic colorectal cancer: results from a large observational cohort study (BRiTE). J Clin Oncol 26(33):5326–5334
6. Ellis LM, Haller DG (2008) Bevacizumab beyond progression: does this make sense? J Clin Oncol 26(33):5313–5315
7. Ince WL, Jubb AM, Holden SN, Holmgren EB, Tobin P, Sridhar M, Hurwitz HI, Kabbinavar F, Novotny WF, Hillan KJ, Koeppen H (2005) Association of k-ras, b-raf, and p53 status with the treatment effect of bevacizumab. J Natl Cancer Inst 97(13): 981–989
8. Hurwitz HI, Yi J, Ince W, Novotny WF, Rosen O (2009) The clinical benefit of bevacizumab in metastatic colorectal cancer is independent of K-ras mutation status: analysis of a phase III study of bevacizumab with chemotherapy in previously untreated metastatic colorectal cancer. Oncologist 14(1):22–28
9. Gordon MS, Cunningham D (2005) Managing patients treated with bevacizumab combination therapy. Oncology 69(Suppl 3):25–33
10. Rini BI (2007) Vascular endothelial growth factor-targeted therapy in renal cell carcinoma: current status and future directions. Clin Cancer Res 13(4):1098–1106
11. Ellis LM (2005) Bevacizumab. Nat Rev Drug Discov Suppl:S8–9
12. Gressett SM, Shah SR (2009) Intricacies of bevacizumab-induced toxicities and their management. Ann Pharmacother 43(3):490–501
13. Chen HX, Cleck JN (2009) Adverse effects of anticancer agents that target the VEGF pathway. Nat Rev Clin Oncol 6(8):465–477
14. Gonzalez-Angulo AM, Hortobagyi GN, Ellis LM (2011) Targeted therapies: Peaking beneath the surface of recent bevacizumab trials. Nat Rev Clin Oncol 8(6):319–320
15. Gerber HP, Wu X, Yu L, Wiesmann C, Liang XH, Lee CV, Fuh G, Olsson C, Damico L, Xie D, Meng YG, Gutierrez J, Corpuz R, Li B, Hall L, Rangell L, Ferrando R, Lowman H, Peale F, Ferrara N (2007) Mice expressing a humanized form of VEGF-A may provide insights into the safety and efficacy of anti-VEGF antibodies. Proc Natl Acad Sci USA 104(9):3478–3483
16. Salomon DS, Brandt R, Ciardiello F, Normanno N (1995) Epidermal growth factor-related peptides and their receptors in human malignancies. Crit Rev Oncol Hematol 19(3):183–232
17. Lurje G, Lenz HJ (2009) EGFR signaling and drug discovery. Oncology 77(6):400–410
18. Tabernero J (2007) The role of VEGF and EGFR inhibition: implications for combining anti-VEGF and anti-EGFR agents. Mol Cancer Res 5(3):203–220
19. Vincenzi B, Zoccoli A, Pantano F, Venditti O, Galluzzo S (2010) Cetuximab: from bench to bedside. Curr Cancer Drug Targets 10(1):80–95. doi:EPub-Abstract-CCDT-12
20. Van Cutsem E, Kohne CH, Hitre E, Zaluski J, Chang Chien CR, Makhson A, D'Haens G, Pinter T, Lim R, Bodoky G, Roh JK, Folprecht G, Ruff P, Stroh C, Tejpar S, Schlichting M, Nippgen J, Rougier P (2009) Cetuximab and chemotherapy as initial treatment for metastatic colorectal cancer. N Engl J Med 360(14): 1408–1417
21. Tol J, Koopman M, Cats A, Rodenburg CJ, Creemers GJ, Schrama JG, Erdkamp FL, Vos AH, van Groeningen CJ, Sinnige HA, Richel DJ, Voest EE, Dijkstra JR, Vink-Borger ME, Antonini NF, Mol L, van Krieken JH, Dalesio O, Punt CJ (2009) Chemotherapy, bevacizumab, and cetuximab in metastatic colorectal cancer. N Engl J Med 360(6):563–572
22. Tabernero J, Cervantes A, Rivera F, Martinelli E, Rojo F, von Heydebreck A, Macarulla T, Rodriguez-Braun E, Eugenia Vega-Villegas M, Senger S, Ramos FJ, Rosello S, Celik I, Stroh C, Baselga J, Ciardiello F (2010) Pharmacogenomic and pharmacoproteomic studies of cetuximab in metastatic colorectal cancer: biomarker analysis of a phase I dose-escalation study. J Clin Oncol 28(7):1181–1189
23. Perrotte P, Matsumoto T, Inoue K, Kuniyasu H, Eve BY, Hicklin DJ, Radinsky R, Dinney CP (1999) Anti-epidermal growth factor receptor antibody C225 inhibits angiogenesis in human transitional cell carcinoma growing orthotopically in nude mice. Clin Cancer Res 5(2):257–265
24. Petit AM, Rak J, Hung MC, Rockwell P, Goldstein N, Fendly B, Kerbel RS (1997) Neutralizing antibodies against epidermal growth factor and ErbB-2/neu receptor tyrosine kinases down-regulate vascular endothelial growth factor production by tumor cells in vitro and in vivo: angiogenic implications for signal transduction therapy of solid tumors. Am J Pathol 151(6):1523–1530
25. Cohen EE, Davis DW, Karrison TG, Seiwert TY, Wong SJ, Nattam S, Kozloff MF, Clark JI, Yan DH, Liu W, Pierce C, Dancey JE, Stenson K, Blair E, Dekker A, Vokes EE (2009)

Erlotinib and bevacizumab in patients with recurrent or metastatic squamous-cell carcinoma of the head and neck: a phase I/II study. Lancet Oncol 10(3):247–257
26. Hecht JR, Mitchell E, Chidiac T, Scroggin C, Hagenstad C, Spigel D, Marshall J, Cohn A, McCollum D, Stella P, Deeter R, Shahin S, Amado RG (2009) A randomized phase IIIB trial of chemotherapy, bevacizumab, and panitumumab compared with chemotherapy and bevacizumab alone for metastatic colorectal cancer. J Clin Oncol 27(5):672–680
27. Verheul HM, Pinedo HM (2007) Possible molecular mechanisms involved in the toxicity of angiogenesis inhibition. Nat Rev Cancer 7(6):475–485
28. Hsu JY, Wakelee HA (2009) Monoclonal antibodies targeting vascular endothelial growth factor: current status and future challenges in cancer therapy. BioDrugs 23(5):289–304
29. Bostrom J, Yu SF, Kan D, Appleton BA, Lee CV, Billeci K, Man W, Peale F, Ross S, Wiesmann C, Fuh G (2009) Variants of the antibody herceptin that interact with HER2 and VEGF at the antigen binding site. Science 323(5921):1610–1614
30. Demicheli R (1980) Growth of testicular neoplasm lung metastases: tumor-specific relation between two Gompertzian parameters. Eur J Cancer 16(12):1603–1608
31. Norton L (1988) A Gompertzian model of human breast cancer growth. Cancer Res 48:7067–7071
32. Magni P, Simeoni M, Poggesi I, Rocchetti M, De Nicolao G (2006) A mathematical model to study the effects of drugs administration on tumor growth dynamics. Math Biosci 200(2): 127–151
33. Panetta JC (1997) A mathematical model of breast and ovarian cancer treated with paclitaxel. Math Biosci 146(2):89–113
34. Simeoni M, Magni P, Cammia C, De Nicolao G, Croci V, Pesenti E, Germani M, Poggesi I, Rocchetti M (2004) Predictive pharmacokinetic-pharmacodynamic modeling of tumor growth kinetics in xenograft models after administration of anticancer agents. Cancer Res 64(3):1094–1101
35. Wang S, Zhou Q, Gallo JM (2009) Demonstration of the equivalent pharmacokinetic/pharmacodynamic dosing strategy in a multiple-dose study of gefitinib. Mol Cancer Ther 8(6):1438–1447
36. Koch G, Walz A, Lahu G, Schropp J (2009) Modeling of tumor growth and anticancer effects of combination therapy. J Pharmacokinet Pharmacodyn 36(2):179–197
37. Magni P, Germani M, De Nicolao G, Bianchini G, Simeoni M, Poggesi I, Rocchetti M (2008) A minimal model of tumor growth inhibition. IEEE Trans Biomed Eng 55(12):2683–2690
38. Tham LS, Wang L, Soo RA, Lee SC, Lee HS, Yong WP, Goh BC, Holford NH (2008) A pharmacodynamic model for the time course of tumor shrinkage by gemcitabine + carboplatin in non-small cell lung cancer patients. Clin Cancer Res 14(13):4213–4218
39. Holt LJ, Herring C, Jespers LS, Woolven BP, Tomlinson IM (2003) Domain antibodies: proteins for therapy. Trends Biotechnol 21(11):484–490
40. Durocher Y, Perret S, Kamen A (2002) High-level and high-throughput recombinant protein production by transient transfection of suspension-growing human 293-EBNA1 cells. Nucleic Acids Res 30(2):E9
41. Zhang X, Zhang H, Tighiouart M, Lee JE, Shin HJ, Khuri FR, Yang CS, Chen ZG, Shin DM (2008) Synergistic inhibition of head and neck tumor growth by green tea (-)-epigallocatechin-3-gallate and EGFR tyrosine kinase inhibitor. Int J Cancer 123(5):1005–1014
42. Shah DK, Veith J, Bernacki RJ, Balthasar JP (2011) Evaluation of combined bevacizumab and intraperitoneal carboplatin or paclitaxel therapy in a mouse model of ovarian cancer. Cancer Chemother Pharmacol. doi:10.1007/s00280-011-1566-3
43. Luo FR, Yang Z, Dong H, Camuso A, McGlinchey K, Fager K, Flefleh C, Kan D, Inigo I, Castaneda S, Rose WC, Kramer RA, Wild R, Lee FY (2005) Correlation of pharmacokinetics with the antitumor activity of Cetuximab in nude mice bearing the GEO human colon carcinoma xenograft. Cancer Chemother Pharmacol 56(5):455–464
44. Thurber GM, Schmidt MM, Wittrup KD (2008) Antibody tumor penetration: transport opposed by systemic and antigen-mediated clearance. Adv Drug Deliv Rev 60(12):1421–1434
45. Beal S, Sheiner LB, Bookman A, Bauer RJ (1989-2009) NONMEM User's Guides. ICON Development Solutions, Ellicott City, MD, USA
46. Zandvliet AS, Schellens JH, Dittrich C, Wanders J, Beijnen JH, Huitema AD (2008) Population pharmacokinetic and pharmacodynamic analysis to support treatment optimization of combination chemotherapy with indisulam and carboplatin. Br J Clin Pharmacol 66(4):485–497
47. Reynolds LM, Infosino A, Brown R, Hsu J, Fisher DM (2000) Pharmacokinetics of rapacuronium in infants and children with intravenous and intramuscular administration. Anesthesiology 92(2):376–386
48. Auerbach R, Auerbach W (1982) Regional differences in the growth of normal and neoplastic cells. Science 215(4529): 127–134
49. Kyriazis AA, Kyriazis AP (1980) Preferential sites of growth of human tumors in nude mice following subcutaneous transplantation. Cancer Res 40(12):4509–4511
50. Ramanathan RK (2008) Alternative dosing schedules for cetuximab: a role for biweekly administration? Clin Colorectal Cancer 7(6):364–368